NUMERICAL FAILURE ANALYSIS OF BUILT-UP COLUMNS COMPOSED OF CLOSELY SPACED PULTRUDED FRP CHANNELS

Fabio MINGHINI[a*], Nerio TULLINI[a], Francesco ASCIONE[b], Luciano FEO[b]

[a] *Engineering Department, University of Ferrara, Via G. Saragat 1, 44122 Ferrara, Italy*

[b] *Department of Civil Engineering, University of Salerno, Via Giovanni Paolo II 132, 84084 Fisciano (SA), Italy*

[a] Corresponding author. E-mail: fabio.minghini@unife.it

ABSTRACT

The results of geometrically nonlinear analyses on 43 built-up Pultruded Fibre-Reinforced Polymer (PFRP) columns with closely spaced chords and intermittent interconnections are presented. A comparison between columns with the end section entirely loaded and columns loaded at the end battens only is reported, showing no appreciable difference in the *P*-δ response. The effects due to variations of column length and battens spacing are then investigated. It is found that stocky columns with small battens spacing attain pre-buckling failure at the web-flange junctions of the chords for loads approximately equal to 70% of the crushing load. Slender columns fail by global buckling, whereas intermediate-slenderness columns may experience interaction between local and global buckling. A design method is finally proposed.

Keywords: PFRP; Built-up columns; Global buckling; Local buckling; Pre-buckling failure; FE analysis

1. INTRODUCTION

Structural engineers are worldwide becoming increasingly aware of the potential of Pultruded Fibre-Reinforced Polymer (PFRP) profiles. However, to promote a widespread use of PFRPs in the

construction industry, there is the need to gain a further insight into their structural performance and develop a comprehensive set of design recommendations.

Built-up members comprised of thin-walled profiles are of common use in steel construction. Similarly, in PFRP structures standard pultruded shapes such as channels and angles are often assembled by bolting or adhesive bonding to obtain built-up beams or columns with improved stiffness. Only to mention a few examples, Pontresina Footbridge [1], built in 1997 and representing one of the first examples of all-FRP structure in Europe, has two truss girders with built-up chords composed of two back-to-back channels [2, 3]. The structural skeleton of the Eyecatcher Building [1], built in 1999 and still remaining the tallest FRP building in the world, is comprised of three parallel trapezoidal pultruded frames whose members were obtained assembling individual standard PFRP shapes by continuous bonding [3, 4]. The arches of the 38 m-span Lleida Footbridge [5], built in 2001 across a roadway and railway line, present a rectangular hollow cross-section obtained from two channels joined with glued flat plates. Back-to-back PFRP channels and angles were used for columns and truss beams, respectively, of the modular all-FRP structure described in [6, 7], designed for a temporary fair stand. In the large pultruded shelter described in [8], accomodating the restoration activities of the church of Santa Maria Paganica in L'Aquila, Italy, built-up PFRP profiles obtained by bolting four channels to one another were adopted.

Despite the frequent use of built-up PFRP members in structures, the research on them still remains at an early stage. Four-point bending test results on profiles analogous to those adopted in the Eyecatcher Building are reported in [4]. An experimental investigation on I-section beams obtained assembling pultruded panels is reported in [9]. Built-up columns analogous to those used in the pultruded shelter described in [8] were analyzed in [10–14]. In particular, in the concentric compression test results presented in [12], the influence of the mode of application of the compressive load was investigated. At equal cross-section area, colums with the compression applied to the whole end sections showed a greater ultimate load than columns with the axial load acting on the two internal channels only. In the former case, the interaction between global and local buckling modes

played a key role in triggering the failure. In the latter case, local failure of the internal channels was observed in proximity of the end sections. Closed-form equations, such as (1) Euler's and (2) Engesser's formulae (applied to the built-up columns considered as members with uniform cross-section) and (3) equations suited for built-up steel columns, did not provide accurate predictions of the buckling load. To capture the actual column behaviour, it was therefore suggested to perform geometrically nonlinear finite element (FE) analyses. Material limiting strength was not considered in these analyses, since they were mainly focused on buckling.

Specific design rules for built-up steel members are available for quite some time now (see for example Section 6.4 of [15]). Conversely, no information for the design of built-up PFRP members is provided by the most up-to-date European design guide for FRP composite structures [16]. Some operative recommendation is provided instead by the design guide published by the ASCE [17]. However, due to the lack of experimental data on built-up PFRP members, the provisions given in [17] are explicitly adapted from the recommendations of the AISC construction manual for steel members [18].

In this paper, a numerical investigation on built-up PFRP columns is reported with the aim of developing specific design rules for these members. The columns analyzed are comprised of two closely spaced back-to-back channels assembled together using pultruded battens. A total of 43 FE models are developed by varying column length and battens spacing. For each of these models, the ultimate compressive load is obtained from a geometrically nonlinear analysis. Material limiting strengths are accounted for in the study using a modified Von Mises failure criterion suitable for web-flange junctions. Previous studies [4, 19–23], indeed, have shown that the resin rich zones at the intersection between pultruded panels often show smaller strengths compared with those of webs and flanges, and may therefore represent the 'weak link in the chain' from which failure starts to propagate. To interpret the numerical results, a slenderness parameter is defined combining the formulation for built-up battened steel columns [24] with that for pultruded I-section columns [22,

25–27]. Finally, it is proposed to use such a slenderness parameter in a design equation analogous to that available for standard PFRP shapes.

For clarity, all symbols used in the text are defined in a Notation section at the end of paper.

2. OUTLINE OF THE RESEARCH

The present paper addresses the Ultimate Limit State (ULS) design of built-up PFRP columns comprised of closely spaced profiles. This Section describes the columns investigated and reports a brief summary of the research. The order of the following subsections reflects the logical order of the research activities.

2.1. Geometric and mechanical properties of the built-up columns

The thin-walled profiles considered in this study are channels (Fig. 1a) with nominal cross-section dimensions 203 × 55.6 × 9.5 mm. The geometric characteristics of the channel section are reported in Table 1.

The built-up columns investigated are comprised of two back-to-back channels (Fig. 1b) connected with one another by means of a certain number, say n, of PFRP battens with nominal dimensions 184 × 50.8 × 12.7 mm (Table 2) and spacing c (Fig. 1c). Two of the n battens are always placed at the column ends. It is assumed that the battens are adhesively bonded to the webs of the channels. Were bolted connections considered instead, different local effects could in theory be expected. However, these effects could be minimized, and then have only a marginal impact on the overall column behaviour, by increasing the number of bolts per batten, so approaching the case of a bonded connection. In any case, the analysis of bolt-induced local effects is out of the scope of the present paper, which is rather aimed at investigating the role of battens spacing on column failure. The geometric characteristics, reported in Table 2, of the built-up ("bu") column cross-section are computed from the following relations: $A_{bu} = 2A_1$, $I_0 = A_{bu}d^2/4$, $I_{bu} = I_0 + 2I_{1,min}$ and $i_{bu} = (I_{bu}/A_{bu})^{0.5}$.

The stiffness properties of the PFRP materials used for channels and battens are reported in Tables 3 and 4, respectively (see [28]). With regard to the channels, transverse elastic moduli different for tension and compression can be noted in the table. In a locally buckled column, webs and flanges of the channels are expected to experience transverse flexure. Therefore, a transverse modulus averaged between tension and compression (E_T) is used in the analyses presented in the following. Alternatively, the transverse flexural modulus provided by the pultruder, about 10% smaller than E_T, could be used.

It is assumed that the pultrusion direction for the battens is parallel to the channels transverse direction. Anyway, no particular influence of the battens orientation relative to the channels has been observed in the numerical analyses.

2.2. Parametric FE analysis

A total of 43 FE models of built-up PFRP columns are developed by varying:

- column length L between 350.8 and 3055.6 mm, and then global slenderness λ_{gl} between 14 and 124;
- battens spacing c between 100 and 1200 mm, leading to $7 \leq \lambda_1 \leq 80$;

A change in L with c kept constant, as well as a change in c at equal L, will imply a different number of battens n (see Fig. 1c). Global and local slendernesses and number of battens are obtained from:

$$\lambda_{gl} = L/i_{bu} \tag{1}$$

$$\lambda_1 = c/i_{1,min} \tag{2}$$

$$n = 1 + \frac{(L - b_{bat})}{c} \tag{3}$$

The generic FE model will be denoted by a label of the form B*pq*-S*rs*, where *p*, *q*, *r* and *s* are digits. In particular, *pq* and *rs* correspond to number of battens ("B") and local slenderness λ_1 ("S"),

respectively. For example, the FE model of a column with length $L = 2050.8$ mm and battens spacing $c = 250$ mm is characterized by $n = 9$ and $\lambda_1 = 17$, and will then be denoted as B09-S17.

A geometric imperfection in the form of a global out-of-straightness in the minor-axis plane is applied to each FE model. A displacement-controlled geometrically nonlinear analysis is then carried out up to material or buckling failure, whichever occurs first.

2.3. Proposal of a design method

A new slenderness parameter λ_P for built-up PFRP columns is defined based on reference loads P_{st} and P_{sl} for stocky and slender columns. In particular, P_{sl} is derived from the theory for built-up steel columns with closely spaced chords [24], whereas P_{st} takes account of local buckling and material limiting strengths. For each of the columns investigated, the FE computed ultimate load, P_u, is then reported in nondimensional form versus λ_P and compared with function $\chi_P(\lambda_P, c_P)$ defined in [25] for standard PFRP shapes with doubly-symmetric cross-section (see also [16, 22, 27]), where $c_P \leq 1$ indicates a shape coefficient. This function represents a family of design curves approaching asymptotically 1 and P_{sl}/P_{st} for stocky and slender columns, respectively. It is shown that using function χ_P for built-up PFRP columns still is possible, and this would allow to predict the ultimate column load as $\chi_P P_{st}$.

3. GEOMETRICALLY NONLINEAR FE ANALYSIS

This Section illustrates the characteristics of the FE models developed and focuses the numerical results obtained.

3.1. Description of the FE models

The FE models are implemented into a multi-purpose software package [29] using orthotropic four-node quadrilateral elements for the channels and eight-node solid elements for the battens. All

plates are oriented so as to align the pultrusion direction for the channels with global z-axis (Fig. 1c). The pultrusion direction for the battens is instead aligned with global y-axis.

3.1.1. FE mesh

In order to avoid overlapping between flanges and webs of the channels at the web-flange junctions and between channels and battens along the column cross-section depth, the meshes of the two thin-walled profiles are located on the inner surfaces of the webs and flanges (see Fig. 2a). For each wall segment of the channels, the mesh location is obtained by defining an offset equal to one half of the actual wall thickness. This expedient, also applied in [20] to the FE analysis of PFRP I-section columns, ensures great accuracy in reproducing the actual cross-sectional area and second moments of area of the column.

A detail of the FE discretization is depicted in Fig. 2b, where the meshes of flanges, webs and batten plates are represented in red, blue and black, respectively. In particular, $n_f = 6$ and $n_w = 22$ subdivisions are initially defined for flanges and webs, respectively, leading to $e_f = B/n_f = 9.27$ mm and $e_w = (H - 2t)/n_w = 8.37$ mm ($e_f/e_w = 1.1$). However, based on the findings reported in [4, 19, 20], the ultimate conditions for stocky columns are expected to be governed by material failure at the web-flange junctions. Therefore, in view of a post-processing check of the material limiting stress state, a mesh refinement is performed by halving the dimensions e_f and e_w of the elements nearest to the web-flange junctions (Fig. 2b). In conclusion, 7 and 24 subdivisions are used for each of the flanges and webs, respectively, resulting in a total of 52 subdivisions on the cross-section plane.

In correspondence of the battens, the meshes of the webs are connected with solid elements with in-plane dimensions $e_w \times (t_{bat}/2)$ far from the web-flange junctions and $(e_w/2) \times (t_{bat}/2)$ in their proximities (Fig. 2b).

The length-wise mesh size e_L is chosen so as to give an aspect ratio e_L/e_w approximately unitary.

Preliminary convergence-rate tests conducted with eigenvalue analyses (linear buckling) confirmed that the mesh sizes adopted ensure a convergent numerical solution.

3.1.2. Constraints

For all analyses described in the following, rigid links are used to enforce planarity of the column end sections (Fig. 3a). This constraint is typical of laboratory compression tests, where rigid plates are generally used to transfer the compressive loads at the ends. Moreover, the columns are assumed simply supported at the end sections. This constraint is reproduced in the FE models by suppressing the displacements of the webs, flanges and battens in the planes of the end sections, whilst the same sections are left free to rotate about their principal inertia axes.

In truss structures, it is frequent that the axial load is transferred to each of the various members through gusset plates located at the end connections. In this case, therefore, the end sections of the member are not entirely loaded. To reproduce this design situation, some of the models is re-analyzed with rigid links which stiffen the end battens only (see Fig. 3b). In these models, the compressive load is then directly applied to the end battens and not to the whole end sections. An analogous comparison between different modes of application of the compressive load was reported in [12], where tests on built-up PFRP columns comprised of four channels were presented.

3.1.3. Geometric imperfection

An investigation on the influence of the imperfection shape on buckling and postbuckling of PFRP I-section columns is reported in [22]. In that study, it was shown that the unintended nonorthogonality between the web and flange panels has no noticeable effect on the ultimate column load. Moreover, imperfections as a global minor-axis out-of-straightness [26, 30] provided column resistances that were on the safe side compared with those obtained in the presence of a local imperfection, analogous to that used by Turvey and Zhang [20] for stocky columns. To

investigate the lateral-torsional buckling of PFRP I-beams, the effects due to minor-axis out-of-straightness and nonorthogonality between web and flange panels were considered in [31]. In [32] it was suggested to take account of a single dominant imperfection with appropriate magnitude. Therefore, in [23], to analyze PFRP I-beams in major-axis bending, only a beam out-of-straightness in the minor-axis plane was considered. Analogously, in the present paper a global minor-axis out-of-straightness is applied to the built-up columns investigated.

Using forces to reproduce the geometric imperfection is generally accepted [22, 23, 32], because the induced initial stress state is generally negligible. In this paper, the global out-of-straightness is reproduced by applying two equal and opposite bending moments $M_{0,y}$ to the master nodes of the rigid links at the end sections (Fig. 3), i.e., the end section centroids. These moments result in a uniform column bending into the minor-axis plane. The values of $M_{0,y}$ are chosen so as to give mid-height deflection $\delta = L/2000$. This imperfection amplitude is close to the upper bound of the out-of-straightnesses reported in [26] for twelve PFRP I-section shapes (L/1800) and more than twice greater than the maximum of the imperfection measurements reported in [30] (L/4500). Greater imperfection amplitudes are not explored because it is believed that in a built-up column the effects of the imperfections of the chords mutually compensate for one another.

3.1.4. Incremental axial shortening

In the nonlinear analyses, the displacement control is used to capture possible softening branches in the load path. In particular, whilst the geometric imperfection is kept unchanged, an incremental column shortening is applied to the end section centroids (black arrow parallel to the column axis in Fig. 3), and from there transferred to all nodes connected with the centroids through the rigid links. This obviously corresponds to define, at each end section, a constraint translating in the axial direction. At each increment, the column axial load is given by the reaction of the translating constraint.

3.2. Ultimate load identification

Many research results are available on PFRP I-section columns. In particular, stocky columns typically fail by local buckling [33] followed by material failure at the web-flange junctions [20]. The corresponding load-displacement plot generally is monotonic up to the onset of failure, with which ultimate column load, namely P_u, is associated. Web-flange separation was also observed in locally buckled I-section beams [19].

Intermediate-slenderness columns tend to suffer from the interaction between local and global buckling modes [34]. In this case, the load-displacement plot loses monotonicity when the principal load path intersects a secondary, descending path and P_u corresponds to the maximum of the curve.

Finally, slender columns typically fail by global buckling [35]. In this case, the load-displacement response shows a long plateau with almost constant load, approaching the buckling load provided by Euler's formula. Crushing failure at the tip of the flanges may also be observed for very large deflections.

For the built-up PFRP beams tested in [4], for which lateral supports were used to prevent lateral-torsional buckling, pre-buckling failure with web-flange separation was observed. It can then be argued that the relatively high stiffness of the built-up members, increased with respect to that of the standard shapes they are comprised of, may lead material failure to anticipate any form of buckling.

Based on the above-mentioned researches, two different ways are used in this paper to identify P_u from the FE analyses of built-up PFRP columns with closely spaced channels. In particular, the ultimate conditions are alternatively associated to material or buckling failure.

To verify the attainment of material failure, the following modified Von Mises criterion is considered for the PFRP material (see [20]):

$$\left(\frac{f_{\mathrm{Lc,FE}}}{f_{\mathrm{Lc}}}\right)^2+\left(\frac{f_{\mathrm{Tt,FE}}}{f_{\mathrm{Tt}}}\right)^2+\left(\frac{f_{\mathrm{Tf,FE}}}{f_{\mathrm{Tf}}}\right)^2+\left(\frac{f_{\mathrm{V,FE}}}{f_{\mathrm{V}}}\right)^2=1, \tag{4}$$

where index "FE" stands for FE analysis result. This criterion is used to check the stress state in the web-flange junctions of the channels, which are believed to be the more vulnerable parts of the built-up columns. An analogous criterion was applied in [4] to built-up beams used in the Eyecatcher Building.

Since the present paper is focused on a merely numerical investigation, no experimental test, specific for the channel section investigated, is carried out to determine the various material strengths involved in the failure criterion of Eq. (4). The strengths reported in Table 5, provided in [28], are used instead. It is worth noting that these strengths were obtained by the pultruder from tests on coupons cut out from web and flange panels and not from tests specifically conceived for web-flange junctions (see [20] and references cited therein).

For the built-up columns tested in [10], when the load was applied to the inner channels only, material failure localized near the end sections of these profiles was observed, leading to a global response significantly different than that obtained for columns with the end sections entirely loaded. In analogy with these findings, for the built-up columns investigated in the present paper, local failure in the end batten plates should be expected when the axial load is applied to them and not to the whole end sections. However, no failure criterion is used for the battens, because in real structures they can be strengthened to avoid their premature failure.

Because the reported failure criterion is not implemented into the commercial software used for the FE analyses, the stress checks are carried out as a post-processing operation. At the onset of failure, i.e., whenever Eq. (4) is satisfied, it is assumed that P_u is achieved.

With regard to columns failing by buckling, two different types of P-δ plots are expected. For columns displaying a global deflected shape into the minor-axis plane and characterized by a long, substantially constant plateau in the P-δ plot, the ultimate conditions are governed by global buckling. As mentioned above, compression failure may be attained in the flanges at very large displacements. However, attaining these so large displacements in the FE analyses is not necessary to identify P_u, because the load does not vary appreciably within the plateau. Finally, when the P-δ

plot is non-monotonic P_u is identified with the peak load, corresponding to a deformed shape involving simultaneously global and local buckling.

3.3. Preliminary linear local buckling analysis

Linear buckling analyses are first carried out to evaluate the local buckling load of the built-up columns. In these analyses, in addition to the constraints described in Section 3.1.2, the web-flange junctions of the channels are restrained to remain straight, which is a typical assumption of local buckling analyses [36, 37]. Moreover, a uniform compressive stress is applied to the end sections instead of the incremental axial shortening, and no imperfection is considered.

The FE computed local buckling load in the absence of battens is $P_{loc,2C}$ = 613 kN. When intermittent interconnections are present between the channels, they stiffen the webs of the channels leading to a greater local buckling load. The local buckling load is weakly influenced by the column length and strongly influenced by the battens spacing, as illustrated in Fig. 4. For each of the investigated values of λ_1, the minimum local buckling load, corresponding to the greatest column length, is reported in the figure in nondimensional form. Load P_{loc} tends to $P_{loc,2C}$ for very large values of λ_1. For example, an increase of λ_1 from 7 to 80 is needed to obtain a reduction of $P_{loc}/P_{loc,2C}$ from 2.83 to 1.04. For $\lambda_1 < 13$ the local buckling load exceeds crushing load $P_R = f_{Lc}A_{bu}$ = 1451 kN. Therefore, for short columns with small battens spacing, a pre-buckling failure is expected.

3.4. Analysis results and discussion

In this Section the main results obtained from the nonlinear FE analyses are reported and commented. Symbol δ is used in the following to identify, with regard to global axes shown in Fig. 1b, c, the minor-axis displacement experienced by the node of coordinates $[\pm t_{bat}/2 \quad 0 \quad L/2]$. In particular, the node belonging to the channel subjected to the greatest axial compression is selected.

In built-up columns with intermittent chord interconnections, such as the batten plates considered in the present investigation, transverse displacements of the chords of opposite signs could in theory arise between two consecutive interconnections. The effects due to the contact between the chords should be taken into account when the sum of the absolute values of these displacements equals the gap between the chords. In [10, 12], contact elements were used to reproduce this feature. In the present study, in order not to increase the computational effort, no contact element is used between the webs of the channels. However, for all models investigated it is verified that, up to the value of δ attained in the analysis, the sum of the displacements of the chords toward one another does not exceed t_{bat}.

The analysis results are summarized in Table 6. For all built-up columns investigated, rigid links stiffening the whole end sections (Fig. 3a) are used. However, for three of the columns a comparison between the rigid link configurations illustrated in Fig. 3 is carried out. The corresponding *P*-δ plots are reported in Fig. 5. For a stocky column with $L = 750.8$ mm (Fig. 5a), achieving material failure according to Eq. (4), defining the rigid links as in Fig. 3b leads to a value of P_u only 3% smaller than loading the whole end sections as in Fig. 3a. For more slender columns with $L = 1250.8$ and 1950.8 mm (Fig. 5b), failing by buckling, no appreciable difference is observed between the two rigid link configurations.

Material failure is attained for ten of the 43 columns analyzed, having $L \leq 1050.8$ mm and $\lambda_l \leq 20$. For columns with $\lambda_l > 20$ only buckling failure is observed.

The interaction between global and local buckling is observed for some of the columns. For example, for columns B13-S07 (Fig. 5b) and B03-S33 (Fig. 6a) a non-monotonic *P*-δ plot is obtained (Fig. 6a), indicating the intersection between an ascending and a descending load paths. The deformed shape corresponding to peak load P_u clearly shows column deflection in the minor-axis plane combined with local flange buckling (Fig. 6b).

The influence of the battens spacing is highlighted in Figs. 7a and 7b for columns with $L \approx 950$ and 2450 mm, respectively. In particular, for the shortest columns (Fig. 7a), chord local slendernesses $\lambda_1 = 30$, 20 and 15, compared with $\lambda_1 = 7$, lead to reductions of P_u of 34%, 21% and 14%, respectively. For the longest columns (Fig. 7b), local slendernesses $\lambda_1 = 80$, 27 and 13 yield column resistances which are 29%, 8% and 2% smaller, respectively, than that obtained for $\lambda_1 = 7$. According to Eurocode 3 [15], built-up steel columns with closely spaced chords should be checked for buckling as a single integral member, provided that the battens spacing meets the requirement $c \leq 15 i_{1,min}$ ($\lambda_1 \leq 15$). Given the influence of λ_1 shown in Fig. 7, it can be concluded that such a provision cannot be applied to short built-up PFRP columns with $L \leq 950$ mm ($\lambda_{gl} \leq 40$), whereas still is valid, for practical purposes, for more slender columns with $L \geq 2450$ mm ($\lambda_{gl} \geq 100$).

The greatest ultimate loads are obtained for the shortest columns, which attain material failure. In particular, for the five columns with $L \leq 750.8$ mm ($\lambda_{gl} \leq 30$), $P_u \geq 948$ kN (see columns B04-S07, B06-S07, B08-S07, B04-S13 and B03-S17 in Table 6). The mean ultimate load for these columns is equal to about $0.67P_R = 977$ kN. Therefore, the stress concentrations at the web-flange junctions arising from the load transfer between chords and battens reduces significantly the column resistance compared to the case of uniform compressive stresses. In addition, $0.67P_R/P_{loc,2C} = 1.59$ (Fig. 4), indicating that stocky columns are going to fail by local buckling only for $\lambda_1 \geq 20$, whereas pre-buckling failure is to be expected for smaller local slenderness.

4. DERIVATION OF A DESIGN METHOD

Based on the numerical results presented above, a design method for built-up PFRP columns is suggested in this Section.

4.1. Bleich's formulation for slenderness of built-up steel columns

For built-up steel columns with batten plates, the deflected shape at buckling is assumed to coincide with a half-sine curve:

$$u_x = U_x \sin(\pi z/L), \tag{5}$$

with u_x and U_x being the deflections in the minor-axis plane at the generic position, z, along the column axis and at mid-height, respectively. The elastic critical load for global buckling ("gl") may be written in the form [24]:

$$P_{\mathrm{gl}}^{\mathrm{bu}} = \pi^2 E_{\mathrm{s}} I_{\mathrm{bu}} / (kL)^2 = \pi^2 E_{\mathrm{s}} I_{\mathrm{bu}} / L_0^2 , \tag{6}$$

where E_{s} indicates Young's modulus for steel and buckling length $L_0 = kL$ is proportional to column length L through a coefficient which takes the following form:

$$k = \sqrt{1 + \frac{\pi^2 I_0}{24 I_{\mathrm{1,min}}} \left(\frac{c}{L}\right)^2 + \frac{\pi^2 I_0 c d}{12 I_{\mathrm{bat}} L^2}} , \tag{7}$$

with I_{bat} being the second moment of area of batten plates in the column buckling plane. In Eq. (7), the second and third terms of the radicand depend on the flexibility of chords and batten plates, respectively.

For rigid batten plates, i.e., for closely spaced chords, the third term of the radicand tends to vanish. Therefore, and Eq. (7) reduces to:

$$k = \sqrt{1 + \frac{\pi^2 I_0}{24 I_{\mathrm{1,min}}} \left(\frac{c}{L}\right)^2} \tag{8}$$

Multiplying both sides of Eq. (8) by slenderness λ_{gl} (see Eq. (1)), an equivalent slenderness is obtained in the form:

$$\frac{kL}{i_{\mathrm{bu}}} = \frac{L_0}{i_{\mathrm{bu}}} = \lambda_{\mathrm{gl,eq}} = \sqrt{\lambda_{\mathrm{gl}}^2 + \frac{\pi^2 I_0}{24 I_{\mathrm{1,min}}} \left(\frac{c}{i_{\mathrm{bu}}}\right)^2} \tag{9}$$

Substituting $1/i_{\mathrm{bu}}^2 = A_{\mathrm{bu}} / I_{\mathrm{bu}}$, $I_{\mathrm{1,min}} = A_{\mathrm{l}} i_{\mathrm{1,min}}^2$ and $\lambda_1 = c/i_{\mathrm{1,min}}$ into Eq. (9) yields:

$$\lambda_{\mathrm{gl,eq}} = \sqrt{\lambda_{\mathrm{gl}}^2 + \frac{\pi^2 I_0}{12 I_{\mathrm{bu}}} \lambda_1^2} \tag{10}$$

The elastic global buckling load for a built-up steel column with closely spaced chords may then be expressed in the form:

$$P_{\mathrm{gl}}^{\mathrm{bu}} = A_{\mathrm{bu}} E_{\mathrm{s}} \pi^2 / \lambda_{\mathrm{gl,eq}}^2 \,, \tag{11}$$

with $\lambda_{\mathrm{gl,eq}}$ computed from Eq. (10).

4.2. Proposed slenderness for built-up PFRP columns

For PFRP columns with standard-shape doubly-symmetric cross-section, a nondimensional slenderness parameter is usually defined as [16, 22, 25–27]:

$$\lambda_P = \sqrt{P_{\mathrm{loc}} / P_{\mathrm{gl}}} \tag{12}$$

where P_{loc} and P_{gl} are the local and global buckling loads computed independently on one another. In particular, P_{gl} typically corresponds to flexural buckling in the minor-axis plane and, depending on whether or not the influence of the shear deformation is negligible, may be expressed with Euler' or Engesser's formula [26], i.e.:

$$P_{\mathrm{Eul}} = \pi^2 E_{\mathrm{eff}} I_{\mathrm{min}} / L_0^2 \tag{13}$$

$$P_{\mathrm{Eng}} = P_{\mathrm{Eul}} / [1 + P_{\mathrm{Eul}} / (A_{\mathrm{V}} G_{\mathrm{eff}})] \,, \tag{14}$$

where I_{min} and A_{V} indicate minimum second moment of area and shear area of the profile, respectively, whereas G_{eff} is the effective shear modulus, which can be estimated from full-section tests (see for example [38]). For commercially available glass-fibre reinforced profiles of high slenderness, i.e., profiles which tend to experience a merely global buckling, the shear deformation may be neglected for practical purposes and P_{gl} is typically approximated by Eq. (13) [22].

In this paper, it is proposed to express the nondimensional slenderness for built-up PFRP columns in the following form:

$$\lambda_P = \sqrt{P_{st}/P_{sl}} \tag{15}$$

with P_{st} and P_{sl} being reference failure loads for stocky ("st") and slender columns ("sl"), respectively. In particular, as is shown in Section 3.4 slender columns again fail by global buckling. Therefore, P_{sl} is assumed to coincide with P_{gl}^{bu} obtained from Eq. (11), provided that E_s is replaced with the effective full-section modulus of the pultruded channels (see Table 3), i.e.:

$$P_{gl}^{bu} = A_{bu} E_{eff} \pi^2 / \lambda_{gl,eq}^2 , \tag{16}$$

where $\lambda_{gl,eq}$ still is obtained from Eq. (10). The resulting values of P_{sl} are reported in Table 6 for all of the columns. To account for pre-buckling failure in stocky built-up columns, P_{st} is assumed to take the form:

$$P_{st} = \min\{\alpha_R P_R, P_{loc}\} = A_{bu} \min\{\alpha_R f_{Lc}, f_{loc}\} = f_{st} A_{bu} , \tag{17}$$

where $\alpha_R P_R = \alpha_R f_{Lc} A_{bu}$ is the ultimate column load for material failure, with $P_R = f_{Lc} A_{bu}$ being the crushing load and $\alpha_R \leq 1$ a coefficient accounting for stress concentrations which may affect some part of the column. According to Section 3.4, for the columns analyzed in this paper $\alpha_R = 0.67$.

The local buckling load for the built-up columns under investigation may be estimated in closed-form as twice the local buckling load of one single channel:

$$P_{loc} = A_{bu} f_{loc} = A_{bu} k_{loc} \frac{\pi^2 E_L}{12(1-\nu_{LT}\nu_{TL})} \left(\frac{t}{b_w}\right)^2 , \tag{18}$$

where $b_w = H - t$ indicates the web height referred to the centrelines of the flanges and k_{loc} is a buckling coefficient taking the following expression [37]:

$$k_{loc} = \frac{2}{\sqrt{1+4\pi^2\eta^3/3}} \sqrt{E_T/E_L} + \frac{2\nu_{LT} E_T/E_L + 4(1+4\eta)(1-\nu_{LT}\nu_{TL}) G_{LT}/E_L}{1+4\pi^2\eta^3/3} , \tag{19}$$

with $\eta = b_f/b_w$ and $b_f = B - t/2$. Equation (19) was derived in [37] from a variational formulation applied to a channel section considered as a whole, and not from discrete plate analysis (see for example [36]). Therefore, using Eqs. (18) and (19) does not require independent calculations for

web and flange panels of the column. Two recent papers [39, 40], concerning the local buckling of PFRP I-section profiles in pure bending or axial compression, provided closed-form equations based on a variational formulation analogous to that used to derive Eq. (19).

The local buckling load obtained from Eqs. (18)-(19) is about 13% smaller than $P_{loc,2C}$ = 613 kN. None of these loads takes account of the stiffening effect of the interconnections between the channels and may lead to too conservative local buckling load predictions (Fig. 4). The dependency of P_{loc} on λ_1 should be accounted for in calculating failure load P_{st}. In this paper, in the absence of a closed-form expression for P_{loc} depending on λ_1, the minimum FE computed P_{loc} for each λ_1 is used in Eq. (17). The resulting values of P_{st} are reported in Table 6 for all of the columns.

Substituting Eqs. (16) and (17) into Eq. (15) yields:

$$\lambda_P = \frac{\lambda_{gl,eq}}{\pi}\sqrt{\frac{f_{st}}{E_{eff}}} = \alpha_\lambda \lambda_{gl,eq}\,, \tag{20}$$

with $\alpha_\lambda = \sqrt{f_{st}/(\pi^2 E_{eff})}$. In conclusion, it is proposed to estimate the column slenderness with Eq. (15) or, alternatively, by multiplying Eq. (10), derived in [24] for steel columns, by coefficient α_λ, which depends on failure stress $f_{st} = \min\{\alpha_R f_{Lc}, f_{loc}\}$ for stocky PFRP columns.

For all of the columns investigated, the values of λ_P are reported in Table 6. In the last column of the same table, the FE computed ultimate loads are reported, in nondimensional form, divided by the corresponding values of P_{st}.

4.3. Design curve

The values of P_u/P_{st} are also graphically reported, versus λ_P, in Fig. 8, where they are compared with nondimensional reference loads $P_{st}/P_{st} = 1$ and $P_{sl}/P_{st} = P_{gl}^{bu}/P_{st} = 1/\lambda_P^2$ (see Eq. (15)). It is confirmed that slender columns (say $\lambda_P \geq 2$) follow the global buckling curve and their ultimate load may be predicted using Eq. (16). The five stocky columns for which $\lambda_P \leq 1$, instead, attain pre-buckling failure at a load approximately equal to $P_{st} = 0.67P_R$. Columns of intermediate slenderness

have ultimate loads smaller than the reference loads. It seems therefore logical to introduce, in analogy with PFRP columns with standard-shape doubly-symmetric cross-section [16, 22, 25–27], a family of nondimensional design curves of the form:

$$\chi_P = \frac{\Phi_P - \sqrt{\Phi_P^2 - c_P \lambda_P^2}}{c_P \lambda_P^2}, \tag{21}$$

where $\Phi_P = (1 + \lambda_P^2)/2$ and c_P is a shape coefficient. Equation (21) tends to 1 and $1/\lambda_P^2$ for stocky and slender columns, respectively. The predicted ("pr") column resistance may be expressed as:

$$P_{\mathrm{u,pr}} = \chi_P P_{\mathrm{st}}. \tag{22}$$

Setting $c_P = 0.85$ provides ultimate column loads smaller than all numerical results. The corresponding design curve is reported with a blue solid line in Fig. 8.

5. CONCLUSIONS

Parametric FE analyses of built-up PFRP columns comprised of two closely spaced channels with nominal dimensions 203 × 55.6 × 9.5 mm and back-to-back distance 12.7 mm, interconnected by means of batten plates, are described in this paper. The main findings of the research may be summarized as follows.

Applying the compressive load to the end battens does not imply appreciable differences in the *P*-δ response with respect to the case of load acting on the whole end sections.

The battens spacing has a strong influence on the column behaviour. In particular, the local buckling load obtained from an eigenvalue analysis for local slenderness $\lambda_1 = 80$ is only 37% of that corresponding to $\lambda_1 = 7$. With regard to the results of geometrically nonlinear analyses, the *P*-δ responses of columns with equal lengths but different values of λ_1 are quite different from one another, especially for relatively short columns. The rule of checking for buckling a built-up column as a single integral member provided that $\lambda_1 \leq 15$, which applies to steel structures designed in accordance with [15], can be used only for very slender PFRP columns with $\lambda_{\mathrm{gl}} \geq 100$.

Stocky columns with $\lambda_{gl} \leq 30$ attain pre-buckling failure at the web-flange junctions of the channels. Due to the stress concentrations induced by the battens in the webs of the channels, the ultimate loads for these columns are approximately 70% of the crushing load. Slender columns fail by global buckling. For these columns, the global slenderness and ultimate load may be predicted using the same expressions adopted in the literature for built-up steel columns. Interaction between global and local buckling modes may occur for columns of intermediate slenderness.

Based of the findings of this numerical investigation, a new slenderness parameter λ_P is proposed for built-up PFRP columns (see Eqs. (15) and (20)). This parameter can be used in a design equation (see Eq. (21)) of the same form as that defined in the past for PFRP columns with standard-shape doubly-symmetric cross-section. In the presence of a single dominant geometric imperfection in the form of a minor-axis out-of-straightness not greater than $L/2000$, shape coefficient $c_P = 0.85$ can be adopted in design curve $\chi_P(\lambda_P)$.

The obtained design equation can be applied to built-up PFRP members subjected to prevailing axial compression, such as columns simply supported at the end sections and members belonging to truss structures. Bending, shear, and possibly torsion responses still remain to be investigated to arrive at design equations suitable for built-up PFRP members in framed structures, for which specific analysis tools there exist (see for example [41, 42]).

An experimental validation of this numerical study will be hopefully carried out in the next future.

ACKNOWLEDGEMENTS

The present investigation was developed in the framework of the Research Program FAR 2018 of the University of Ferrara. A special acknowledgement is due to Dr. Fayez Abu Sahyoun for his contribution to the implementation of FE models.

NOTATION

The symbols used in the present paper are defined in the following.

A_{bu}, A_1 = cross-section areas of a built-up column and one of its chords;

B, H, t = cross-section dimensions of one chord;

b_{bat}, h_{bat}, t_{bat} = batten plate dimensions;

b_f, b_w = cross-section dimensions referred to the panels centrelines;

C, C_1 = cross-section centroids;

c = battens spacing;

c_P = buckling mode interaction constant;

d, e = inter-centroidal distance and distance $(d - t_{bat})/2$ (Fig. 1);

E_{eff} = effective Young's modulus;

E_L, E_{Lc}, E_{Lt} = longitudinal average, compressive and tensile moduli;

E_s = Young's modulus for steel;

E_T, E_{Tc}, E_{Tt} = transverse average, compressive and tensile moduli;

E_3 = flatwise Young's modulus for PFRP battens;

e_f, e_w = mesh sizes;

f_{loc}, k_{loc} = local buckling stress and coefficient;

f_{Lc} = longitudinal compressive strength;

f_{Tf}, f_{Tt} = transverse flexural and tensile strengths;

f_V = shear strength;

G_{LT} = in-plane shear modulus;

G_{T3}, G_{3L} = through-the-thickness shear moduli for PFRP battens;

I_{bu}, i_{bu} = second moment of area and radius of gyration of a built-up column;

$I_{1,min}$, $i_{1,min}$ = minimum second moment of area and radius of gyration of one chord;

I_0 = contribution to I_{bu} related with d;

k = (global) buckling length coefficient;

L = column length;

n = number of battens;

P, P_u = compressive axial load and ultimate compressive resistance;

P_{Eng}, P_{Eul} = Engesser' and Euler's buckling loads;

P_{gl}^{bu} , P_{loc} = global buckling load for a built-up column and local buckling load;

P_R = crushing load;

P_{sl}, P_{st} = reference failure loads for slender and stocky columns;

x, y, z = global axes;

α_R = coefficient used to reduce P_R;

α_λ = coefficient relating λ_P with $\lambda_{gl,eq}$;

χ_P = function representing a family of buckling curves;

δ = minor-axis plane mid-height displacement of one column chord;

Φ_P = function of slenderness λ_P;

η = section shape ratio b_f/b_w;

λ_{gl}, $\lambda_{gl,eq}$ = global and equivalent global slendernesses;

λ_P = slenderness parameter for built-up PFRP columns;

λ_1 = chord slenderness $c/i_{1,min}$;

ν_{LT}, ν_{TL} = major and minor Poisson's ratios;

ν_{T3}, ν_{3L} = through-the-thickness Poisson's ratios for PFRP battens.

DATA AVAILABILITY

The data required to reproduce these findings are available to download from https://data.mendeley.com/datasets/rrvpjsrb5w/1 (DOI: 10.17632/rrvpjsrb5w.1).

REFERENCES

[1] Keller T. Recent all-composite and hybrid fibre-reinforced polymer bridges and buildings. *Progress in Structural Engineering and Materials* 2001; 3: 132-140.

[2] Keller T, Bai Y, Vallée T. Long-term performance of a glass fiber-reinforced polymer truss bridge. *Journal of Composites for Construction* 2007; 11(1): 99-108.

[3] Keller T, Theodorou NA, Vassilopoulos AP, de Castro J. Effect of natural weathering on durability of pultruded glass fiber-reinforced bridge and building structures. *Journal of Composites for Construction* 2016, 20(1), 04015025.

[4] Bai Y, Keller T, Wu C. Pre-buckling and post-buckling failure at the web-flange junction of pultruded GFRP beams. *Materials and Structures* 2013; 46: 1143-1154.

[5] Sobrino JA, Pulido MDG. Towards advanced composite material footbridges. *Structural Engineering International* 2002; 12(2): 84-86.

[6] Dicuonzo A, Laudiero F, Minghini F, Tullini N, Maceri F. Design and construction of a temporary structure composed by FRP pultruded profiles. In: Proceedings of the 4th International Conference on FRP Composites in Civil Engineering (CICE), Zürich, 22-24 July 2008.

[7] Minghini F, Tullini N, Ascione F. Updating Italian Design Guide CNR DT-205/2007 in view of recent research findings: Requirements for pultruded FRP profiles. *American Journal of Engineering and Applied Sciences* 2016; 9(3): 702-712.

[8] Russo S. Experimental and finite element analysis of a very large pultruded FRP structure subjected to free vibration. *Composite Structures* 2012; 94(3): 1097-1105.

[9] Ascione F, Mancusi G, Spadea S, Lamberti M, Lebon F, Maurel-Pantel A. On the flexural behaviour of GFRP beams obtained by bonding simple panels: An experimental investigation. *Composite Structures* 2015; 131: 55-65.

[10] Boscato G, Casalegno C, Russo S, Mottram JT. Buckling of built-up columns of pultruded fiber-reinforced polymer C-sections. *Journal of Composites for Construction* 2014; 18(4), 04013050.

[11] Russo S. Investigation on buckling of all-FRP bolted built-up columns. *IES Journal Part A: Civil and Structural Engineering* 2014; 7(3): 174-194.

[12] Boscato G, Casalegno C, Russo S. Performance of built-up columns made by pultruded FRP material. *Composite Structures* 2015; 121: 46-63.

[13] Russo S. Bucklings interactions in columns made by built-up thin, open, pultruded FRP shapes. *Journal of Reinforced Plastics and Composites* 2015; 34(12): 972-988.

[14] Russo S. Shear and local effects in All-FRP bolted built-up columns. *Advances in Structural Engineering* 2015; 18(8): 1227-1240.

[15] European Committee for Standardization. *EN 1993-1-1:2005, Eurocode 3 – Design of steel structures – Part 1-1: General rules and rules for buildings*. Brussels, Belgium, 2005.

[16] Ascione L, Caron J-F, Godonou P, van IJselmuijden K, Knippers J, Mottram JT, Oppe M, Gantriis Sorensen M, Taby J, Tromp L. *Prospect for new guidance in the design of FRP*, EUR 27666 EN, doi: 10.2788/22306.

[17] American Society of Civil Engineers. *Pre-standard for load & resistance factor design of pultruded FRP structures*, 2012.

[18] American Institute for Steel Construction. *Steel construction manual*, 15th Ed., 2017.

[19] Bank LC, Yin J. Failure of web-flange junction in postbuckled pultruded I-beams. *Journal of Composites for Construction* 1999; 3(4): 177-184.

[20] Turvey GJ, Zhang Y. A computational and experimental analysis of the buckling, postbuckling and initial failure of pultruded GRP columns. *Computers & Structures* 2006; 84(22-23): 1527-1537.

[21] Feo L, Mosallam AS, Penna R. Mechanical behavior of web-flange junctions of thin-walled pultruded I-profiles: an experimental and numerical evaluation.

Composites Part B: Engineering 2013; 48: 18-39.

[22] Laudiero F, Minghini F, Tullini N. Buckling and postbuckling finite element analysis of pultruded FRP profiles under pure compression. *Journal of Composites for Construction* 2014; 18(1), 04013026.

[23] Laudiero F, Minghini F, Tullini N. Postbuckling failure analysis of pultruded FRP beams under uniform bending. *Composites Part B: Engineering* 2013; 54: 431-438.

[24] Bleich F. *Buckling strength of metal structures*. New York: McGraw-Hill Book Company, 1952.

[25] Barbero EJ, Tomblin J. A phenomenological design equation for FRP columns with interaction between local and global buckling. *Thin-Walled Structures* 1994; 18(2): 117-131.

[26] Zureick A, Scott D. Short-term behavior and design of fiber-reinforced polymeric slender members under axial compression. *Journal of Composites for Construction* 1997; 1(4): 140-149.

[27] Vanevenhoven LM, Shield CK, Bank LC. LRFD factors for pultruded wide-flange columns. *Journal of Structural Engineering* 2010; 136(5): 554-564.

[28] Creative Pultrusions. *The New and Improved Pultex® Pultrusion Design Manual of Standard and Custom Fiber Reinforced Polymer Structural Profiles*, Vol. 5, Rev. 6. Alum Bank: Creative Pultrusions, Inc., 2017.

[29] STRAND7®. *Theoretical manual—Theoretical background to the Strand7 finite element analysis system*, First ed., 2004.

[30] Mottram JT, Brown ND, Anderson D. Physical testing for concentrically loaded columns of pultruded glass fibre reinforced plastic profile. *Proceedings of the Institution of Civil Engineers, Structures and Buildings* 2003; 158(1): 205-219.

[31] Ascione F. Influence of initial geometric imperfections in the lateral buckling problem of thin walled pultruded GFRP I-profiles. *Composite Structures* 2014; 112: 85-99.

[32] Nguyen TT, Chan TM, Mottram JT. Influence of boundary conditions and geometric imperfections on lateral-torsional buckling resistance of a pultruded FRP I-beam by FEA. *Composite Structures* 2012; 100: 233-242.

[33] Barbero EJ, Raftoyiannis IG. Local buckling of FRP beams and columns. *Journal of Materials in Civil Engineering* 1993; 5(3): 339-355.

[34] Barbero EJ, Dede L, Jones S. Experimental verification of buckling-mode interaction in intermediate-length composite columns. *International Journal of Solids and Structures* 2000; 37(29): 3919-3934.

[35] Barbero EJ, Raftoyiannis IG. Euler buckling of pultruded composite columns. *Composite Structures* 1993; 24(2): 139-147.

[36] Kollár LP. Local buckling of fiber reinforced plastic composite structural members with open and closed cross sections. *Journal of Structural Engineering* 2003; 129(11): 1503-1513.

[37] Cardoso DCT, Harries KA, de M Batista E. Closed-form equations for compressive local buckling of pultruded thin-walled sections. *Thin-Walled Structures* 2014; 79(2): 16-22.

[38] Minghini F, Tullini N, Laudiero F. Identification of the short-term full-section moduli of pultruded FRP profiles using bending tests. *Journal of Composites for Construction* 2014; 18(1), 04013030.

[39] Ascione F, Feo L, Lamberti M, Minghini F, Tullini N. A closed-form equation for the local buckling moment of pultruded FRP I-beams in major-axis bending. *Composites Part B: Engineering* 2016; 97: 292-299.

[40] Cardoso DCT, Vieira JD. Comprehensive local buckling equations for FRP I-sections in pure bending or compression. *Composite Structures* 2017; 182: 301-310.

[41] Minghini F, Tullini N, Laudiero F. Elastic buckling analysis of pultruded FRP portal frames having semi-rigid connections. *Engineering Structures* 2009; 31(2): 292-299.

[42] Minghini F, Tullini N, Laudiero F. Vibration analysis of pultruded FRP frames with semi-rigid connections. *Engineering Structures* 2010; 32(10): 3344-3354.

Figure Captions

Fig. 1. Cross-sectional view of (a) one single channel and (b) two back-to-back channels connected through a batten plate; (c) side view of a built-up member.

Fig. 2. FE model of a built-up column with the mesh located on the inner surfaces of the webs and flanges: (a) general and (b) detail views of the cross-section.

Fig. 3. Isometric view of a FE model: rigid links stiffening (a) the whole end section and (b) the end batten plate only. The black arrow at the centroid of the end section indicates the imposed longitudinal translation (global axes shown).

Fig. 4. FE computed, nondimensional local buckling load versus λ_1.

Fig. 5. FE computed P-δ plots: (a) column B08-S07; (b) columns B13-S07 and B20-S07. Comparison between the rigid link configurations shown in Figs. 3a (blue solid line) and 3b (red symbols).

Fig. 6. Column B03-S33: (a) FE computed P-δ plot and (b) deformed shape at peak load P_u, with interaction between global and local buckling modes.

Fig. 7. FE computed P-δ plots: (a) columns B10-S07 ($\lambda_1 = 7$), B05-S15 ($\lambda_1 = 15$), B04-S20 ($\lambda_1 = 20$) and B03-S30 ($\lambda_1 = 30$) with $L \approx 950$ mm; (b) columns B25-S07 ($\lambda_1 = 7$), B13-S13 ($\lambda_1 = 13$), B07-S27 ($\lambda_1 = 27$) and B03-S80 ($\lambda_1 = 80$) with $L \approx 2450$ mm.

Fig. 8. FE computed, nondimensional ultimate loads (red symbols) compared with the theoretical reference loads for stocky and slender columns (black lines) and the buckling interaction design curve obtained for $c_P = 0.85$ (blue line).

Table Captions

Table 1. Geometric characteristics of one single channel section.

Table 2. Geometric characteristics of battens and built-up column cross-sections comprised of two back-to-back channels.

Table 3. Stiffnesses of the PFRP channels investigated.

Table 4. Stiffnesses adopted for the PFRP battens.

Table 5. Strengths used in the modified Von Mises criterion.

Table 6. Geometric characteristics, reference loads P_{sl} and P_{st}, FE computed ultimate load P_u and failure mode for the 43 columns investigated.

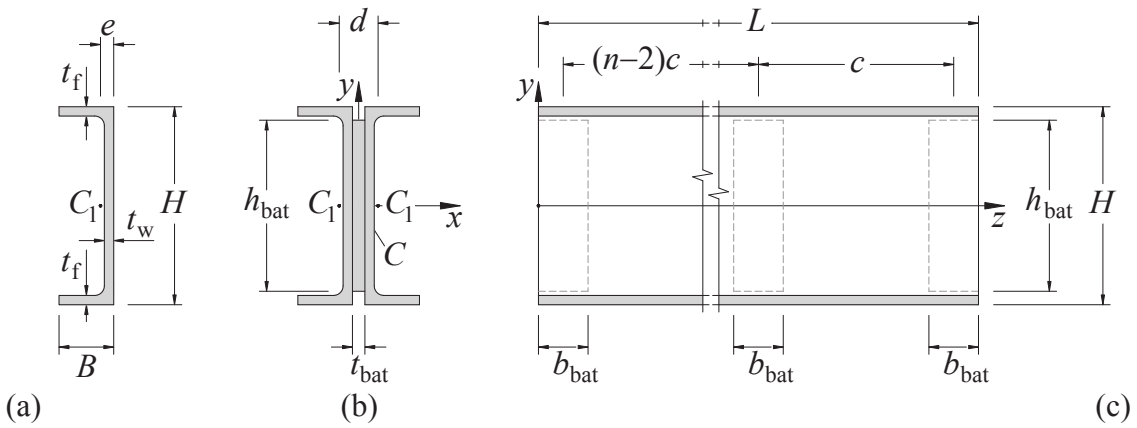

Figure 1. Cross-sectional view of (a) one single channel and (b) two back-to-back channels connected through a batten plate; (c) side view of a built-up member.

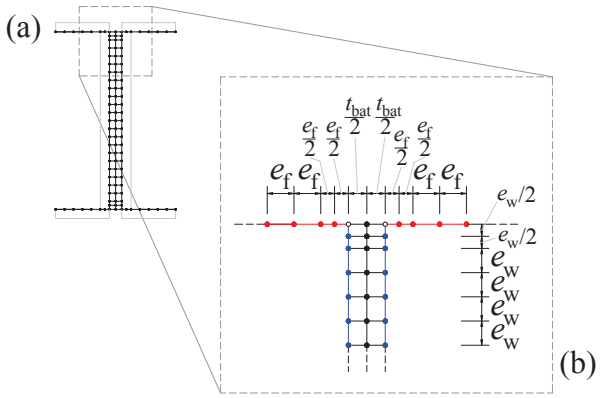

Figure 2. FE model of a built-up column with the mesh located on the inner surfaces of the webs and flanges: (a) general and (b) detail views of the cross-section.

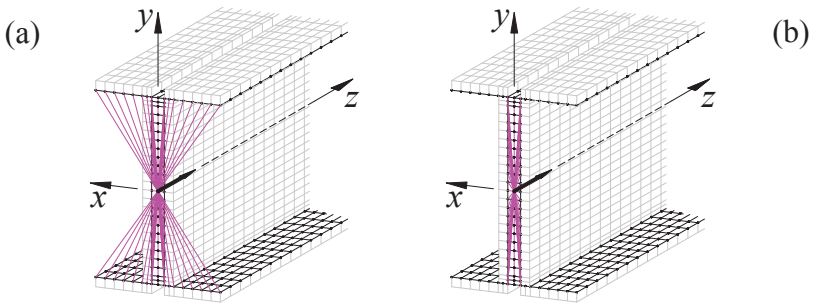

Figure 3. Isometric view of a FE model: rigid links stiffening (a) the whole end section and (b) the end batten plate only. The black arrow at the centroid of the end section indicates the imposed longitudinal translation (global axes shown).

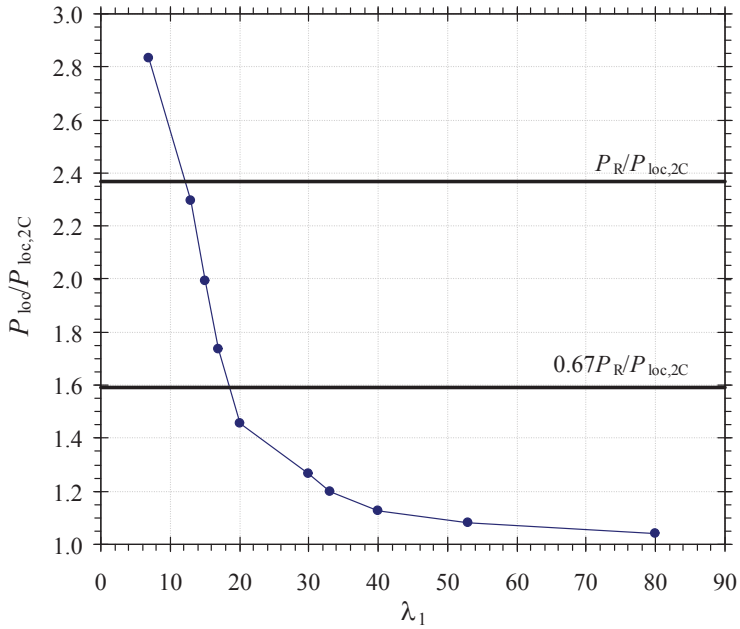

Figure 4. FE computed, nondimensional local buckling load versus λ_1.

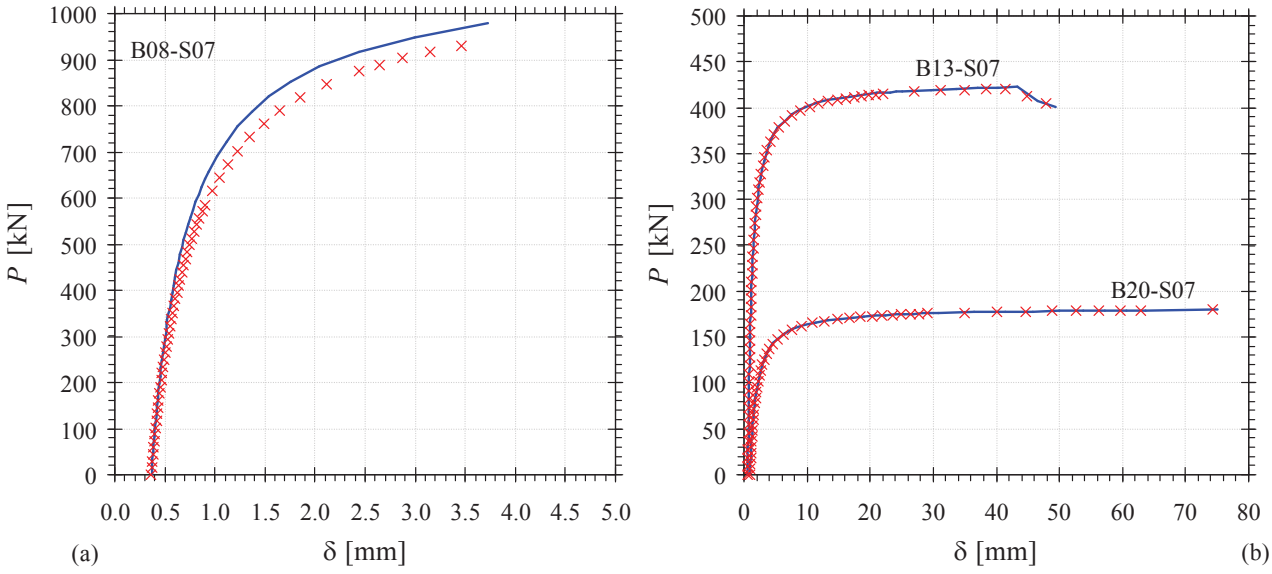

Figure 5. FE computed P-δ plots: (a) column B08-S07; (b) columns B13-S07 and B20-S07. Comparison between the rigid link configurations shown in Figs. 3a (blue solid line) and 3b (red symbols).

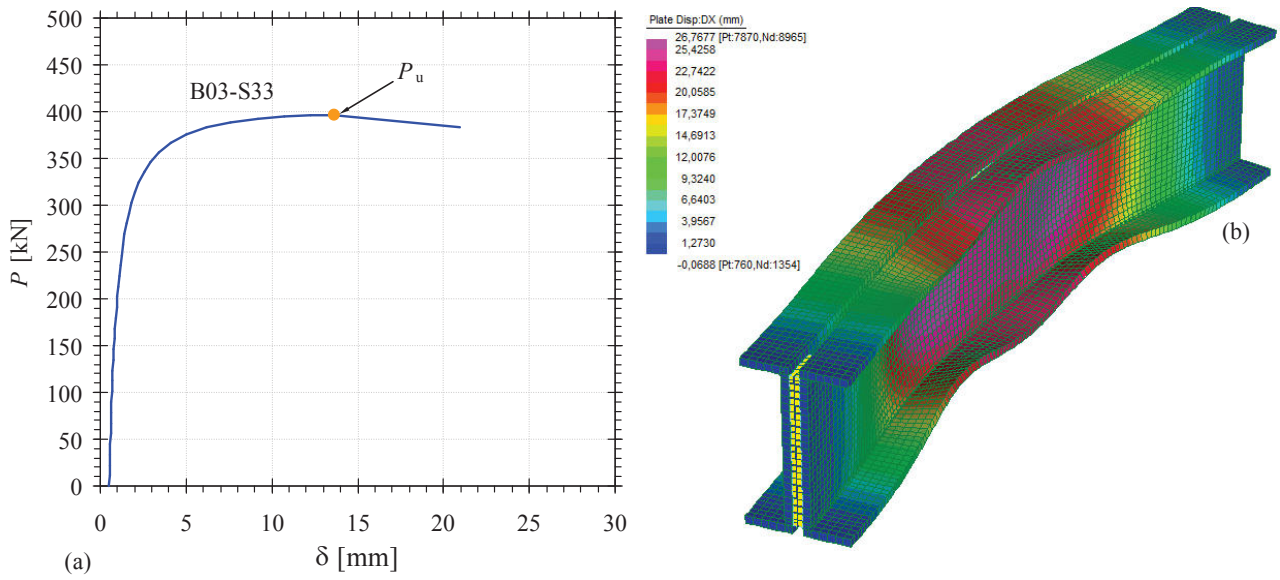

Figure 6. Column B03-S33: (a) FE computed P-δ plot and (b) deformed shape at peak load P_u, with interaction between global and local buckling modes.

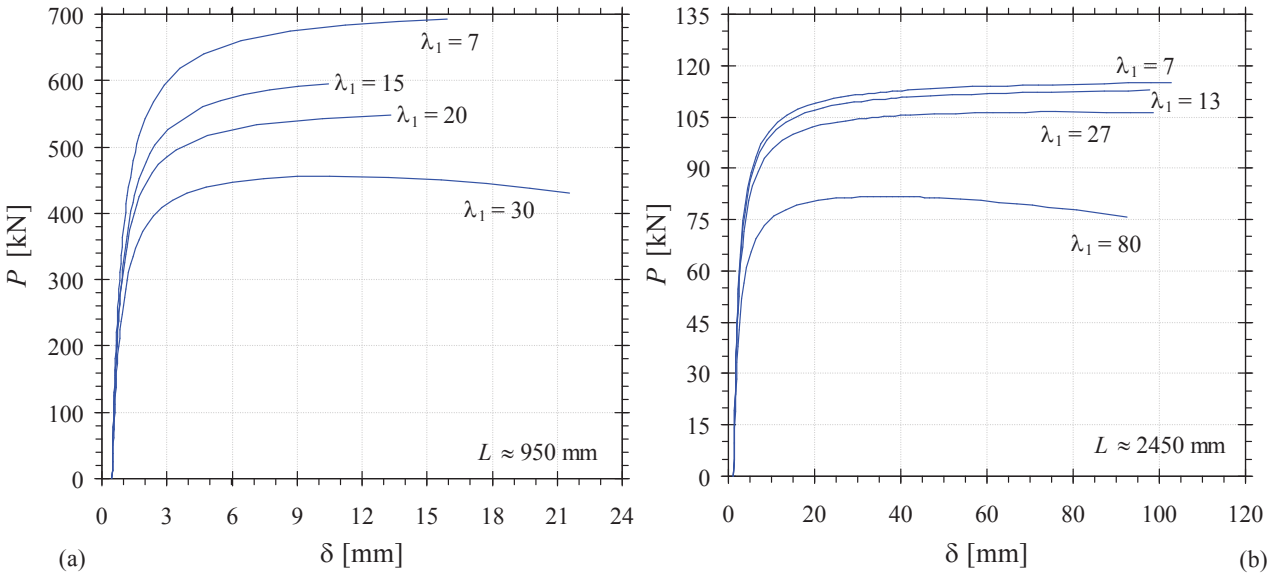

Figure 7. FE computed P-δ plots: (a) columns B10-S07 ($\lambda_1 = 7$), B05-S15 ($\lambda_1 = 15$), B04-S20 ($\lambda_1 = 20$) and B03-S30 ($\lambda_1 = 30$) with $L \approx 950$ mm; (b) columns B25-S07 ($\lambda_1 = 7$), B13-S13 ($\lambda_1 = 13$), B07-S27 ($\lambda_1 = 27$) and B03-S80 ($\lambda_1 = 80$) with $L \approx 2450$ mm.

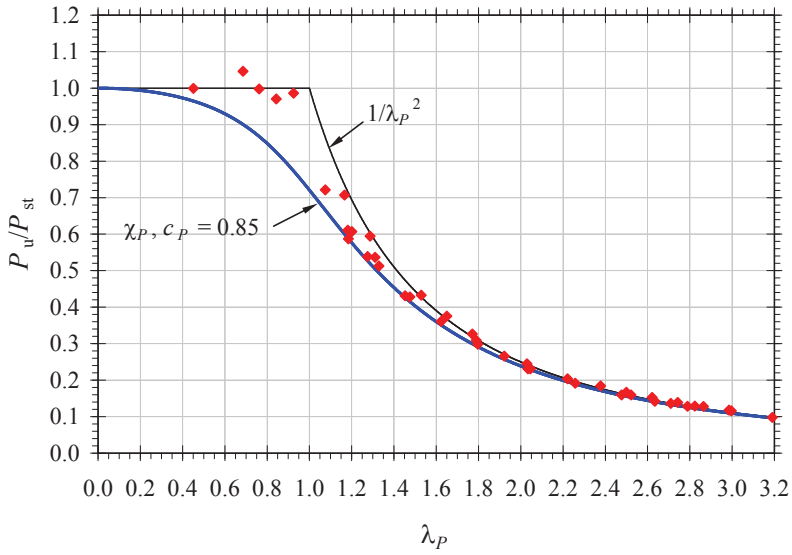

Figure 8. FE computed, nondimensional ultimate loads (red symbols) compared with the theoretical reference loads for stocky and slender columns (black lines) and the buckling interaction design curve obtained for $c_P = 0.85$ (blue line).

Table 1. Geometric characteristics of one single channel section.

H [mm]	B [mm]	$t = t_f = t_w$ [mm]	A_1 [10^3 mm^2]	$I_{1,min}$ [10^5 mm^4]	$i_{1,min}$ [mm]	e [mm]
203.20	55.63	9.53	2.815	6.379	15.05	13.44

Table 2. Geometric characteristics of battens and built-up column cross-sections comprised of two back-to-back channels.

t_{bat} [mm]	b_{bat} [mm]	h_{bat} [mm]	D [mm]	A_{bu} [10^3 mm^2]	I_0 [10^6 mm^4]	I_{bu} [10^6 mm^4]	i_{bu} [mm]
12.70	50.80	184.14	39.59	5.630	2.207	3.482	24.87

Table 3. Stiffnesses of the PFRP channels investigated.

E_{Lt} [GPa]	E_{Lc} [GPa]	E_L [GPa]	E_{Tt} [GPa]	E_{Tc} [GPa]	E_T [GPa]	G_{LT} [GPa]	ν_{LT} [-]	ν_{TL} [-]	E_{eff} [GPa]
20.6	20.6	20.6	6.9	8.2	7.6	2.9	0.35	0.15	19.2

Table 4. Stiffnesses adopted for the PFRP battens.

E_L [GPa]	E_T [GPa]	E_3 [GPa]	$G_{LT}=G_{T3}=G_{3L}$ [GPa]	$\nu_{LT}=\nu_{T3}=\nu_{3L}$ [-]
12.4	6.9	20.6	2.9	0.3

Table 5. Strengths used in the modified Von Mises criterion.

f_{Lc} [MPa]	f_{Tt} [MPa]	f_{Tf} [MPa]	f_V [MPa]
257.8	55.0	85.9	31.0

Table 6. Geometric characteristics, reference loads P_{sl} and P_{st}, FE computed ultimate load P_u and failure mode for the 43 columns investigated.

Analysis No.	Model ID	L [mm]	c [mm]	λ_l [-]	P_{sl} [kN]	P_{st} [kN]	P_u [kN]	Fail. mode*	λ_P [-]	P_u/P_{st} [-]
1	B04-S07	350.8	100	7	4807	977	977	MF	0.45	1.00
2	B06-S07	550.8	100	7	2078	977	1022	MF	0.69	1.05
3	B08-S07	750.8	100	7	1142	977	964	MF	0.93	0.99
4	B10-S07	950.8	100	7	719	977	691	MF	1.17	0.71
5	B11-S07	1050.8	100	7	590	977	581	MF	1.29	0.59
6	B13-S07	1250.8	100	7	418	977	423	BF	1.53	0.43
7	B14-S07	1350.8	100	7	359	977	367	BF	1.65	0.38
8	B15-S07	1450.8	100	7	311	977	319	BF	1.77	0.33
9	B20-S07	1950.8	100	7	173	977	180	BF	2.38	0.18
10	B21-S07	2050.8	100	7	156	977	163	BF	2.50	0.17
11	B22-S07	2150.8	100	7	142	977	149	BF	2.62	0.15
12	B23-S07	2250.8	100	7	130	977	136	BF	2.74	0.14
13	B24-S07	2350.8	100	7	119	977	125	BF	2.86	0.13
14	B25-S07	2450.8	100	7	110	977	115	BF	2.99	0.12
15	B04-S13	650.8	200	13	1374	977	948	MF	0.84	0.97
16	B05-S13	850.8	200	13	845	977	705	MF	1.08	0.72
17	B06-S13	1050.8	200	13	568	977	524	BF	1.31	0.54
18	B08-S13	1450.8	200	13	305	977	302	BF	1.79	0.31
19	B09-S13	1650.8	200	13	237	977	239	BF	2.03	0.24
20	B13-S13	2450.8	200	13	109	977	113	BF	3.00	0.12
21	B05-S15	949.5	225	15	678	977	593	MF	1.20	0.61
22	B03-S17	550.8	250	17	1682	977	975	MF	0.76	1.00
23	B05-S17	1050.8	250	17	553	977	501	BF	1.33	0.51
24	B06-S17	1300.8	250	17	371	977	353	BF	1.62	0.36
25	B07-S17	1550.8	250	17	265	977	260	BF	1.92	0.27
26	B08-S17	1800.8	250	17	198	977	199	BF	2.22	0.20
27	B09-S17	2050.8	250	17	154	977	156	BF	2.52	0.16
28	B10-S17	2300.8	250	17	123	977	126	BF	2.82	0.13
29	B04-S20	950.8	300	20	639	893	546	MF	1.18	0.61
30	B04-S27	1250.8	400	27	368	777	335	BF	1.45	0.43
31	B07-S27	2450.8	400	27	106	777	106	BF	2.71	0.14
32	B05-S29	1810.8	440	29	186	777	180	BF	2.05	0.23
33	B03-S30	950.8	450	30	554	777	456	BF	1.18	0.59
34	B03-S33	1050.8	500	33	452	735	396	BF	1.28	0.54
35	B05-S33	2054.0	501	33	144	735	141	BF	2.26	0.19
36	B07-S33	3055.6	501	33	68	735	68	BF	3.29	0.09
37	B03-S40	1250.8	600	40	318	691	296	BF	1.47	0.43
38	B04-S40	1853.7	601	40	167	691	160	BF	2.03	0.23
39	B03-S50	1553.2	751	50	205	662	198	BF	1.80	0.30
40	B04-S50	2304.4	751	50	108	662	106	BF	2.48	0.16
41	B05-S50	3055.6	751	50	65	662	65	BF	3.19	0.10
42	B04-S53	2450.8	800	53	95	662	94	BF	2.63	0.14
43	B03-S80	2450.8	1200	80	82	637	82	BF	2.79	0.13

* Note: failure modes MF and BF stand for Material Failure and Buckling Failure, respectively.